Influence of Rotation Speed on Microstructure and Mechanical Properties of Friction Stir Lap Welded Joints of AA 6061 and Ti6Al4V Alloys

LI ZHOU, MINGRUN YU, ZHIHUA JIANG, FAN GUO, HONGYUN ZHAO, YONGXIAN HUANG, and XIAOGUO SONG

Three-mm-thick AA 6061 plate and 2-mm-thick Ti6Al4V plate were friction stir lap welded using a W-Re pin tool. Defect-free joints were obtained at various rotation speeds ranging from 800 to 1400 rpm with a constant welding speed of 100 mm/min. The influence of rotation speed on the microstructure and mechanical properties of the Al/Ti friction stir lap welding (FSLW) joints was investigated. At low rotation speed within 1000 rpm, the obtained joint has no obvious mechanical Al/Ti intermixing at the interface. However, a significant mechanical mixture of Al and Ti alloys accompanied by hooks could be found in the joint welded at a rotation speed over 1000 rpm. Only diffusion layer was observed in the joint obtained at low rotation speed. Further, IMCs could be found in the Al/Ti mixture and hook when the rotation speed increased to 1400 rpm. The highest microhardness was measured at the interface due to the formation of IMCs. The tensile shear load of the welded joints reached the maximum at 1000 rpm and the specimens failed along the interface during the test.

I. INTRODUCTION

THE Al/Ti hybrid structure can be widely applied in many fields that need to reduce weight and improve specific strength and comprehensive properties, such as the aerospace and automobile industries, as reported by Simoncini and Forcellese.[1] The joining of Al and Ti dissimilar alloys is essential for the application of the Al/Ti hybrid structure. However, the physical, chemical, and metallurgical differences between them make it a challenge to successfully weld Al/Ti dissimilar alloys.

Fusion welding, brazing, and welding brazing of Al/Ti dissimilar alloys have been investigated in many studies. However, the formation of brittle intermetallic compounds (IMCs) is still an unsolved key problem for Al/Ti welding. In the earlier work of Michael et al.,[2] the formation of brittle IMCs in Al/Ti dissimilar joints is hard to control during laser welding, resulting in precarious mechanical properties. Moreover, different fillers were used to join Al and Ti alloys by brazing to control interfacial reactions. Lv et al.[3] found that proper addition of zirconium in the filler could enhance the mechanical properties of the brazed Al/Ti dissimilar joints. Also, as reported by Chen et al.[4] and Chang et al.,[5] the strength of brazed Al/Ti joints could reach a higher value with proper content of silicon and lanthanide in the filler. Recently, conventional solid-state welding methods, such as diffusion welding and ultrasonic welding, have been attempted to join Al and Ti alloys. However, the brittle IMCs were also formed in the diffusion welded Al/Ti joints, as reported by Alhazaa and Khan.[6] On the other hand, Wang et al.[7] suggested that ultrasonic spot welding could join Al/Ti dissimilar alloys. However, Zhang et al.[8] pointed out that the tensile shear strength of the USW joints was enhanced at first and then remained constant as the welding time reached 2 seconds or more. Furthermore, there are limitations on the geometry of the workpiece and the joining efficiency for the conventional solid-state joining processes.

Friction stir welding (FSW) is a novel solid-state joining process patented by The Welding Institution, which is promising for the joining of dissimilar alloys. So far, many works have been done focusing on friction

LI ZHOU, MINGRUN YU, HONGYUN ZHAO, and XIAOGUO SONG are with the State Key Laboratory of Advanced Welding and Joining, Harbin Institute of Technology, Harbin 150001, P.R. China and also with the Shandong Provincial Key Laboratory of Special Welding Technology, Harbin Institute of Technology at Weihai, Weihai, 264209, P.R. China. Contact e-mail: hy_zhao66@163.com ZHIHUA JIANG and FAN GUO are with the Shandong Provincial Key Laboratory of Special Welding Technology, Harbin Institute of Technology at Weihai. YONGXIAN HUANG is with the State Key Laboratory of Advanced Welding and Joining, Harbin Institute of Technology. Contact e-mail: yxhuang@hit.edu.cn

stir butt welding of Al/Ti dissimilar alloys. Aonuma and Nkata[9] proposed that the formation of IMCs is also a key problem for Al/Ti FSW as well as other welding processes. Wu et al.[10] further found that Al melting significantly weakened the FSW joints of Al and Ti alloys. Li et al.[11] explored that a diffusion layer, instead of the IMC layer, can be found in the joint with proper parameters, which could promote the tensile strength of the joint. Furthermore, Bang et al.[12] found that shifting the probe toward the Al side could enhance the intermixing and material flow of Al and Ti alloys without Al melting in FSW. So far, a few reports about friction stir lap welding (FSLW) of Al and Ti alloys have been reported. Chen and Nakata[13] pointed out that TiAl$_3$ formed at the Al/Ti interface by means of diffusion in the FSLW Al/Ti joints, and the amount of the Al-Ti IMC was significantly affected by heat input during welding. Chen et al.[14] suggested that the intermixing of base materials can be found at the interface accompanied by hooks in the Al/Ti FSLW joint. In addition, Al-Ti IMCs were considered to form at the interface as well as at the edge of the hook structure, as reported by Li et al.[15] However, as investigated by Chen and Yazdanian,[16] either the microstructure or maximum tensile-shear load along the friction stir lap weld of Al and Ti alloys is not homogeneous, and the highest load of 703 N/mm is obtained using a threaded pin tool with a diameter of 6 mm.

Although several studies about FSLW of Al and Ti alloys mentioned previously have been conducted, systematic research about the influence of process parameters on the FSLW joint is limited. In the present study, Al alloy AA 6061 and Ti alloy Ti6Al4V are welded by FSLW. Also, the effect of rotation speed on microstructural characterization and mechanical properties of weld joints is studied. Furthermore, the joining mechanism of FSLW of Al/Ti dissimilar alloys is revealed.

II. MATERIALS AND EXPERIMENTAL PROCEDURE

The as-received materials are 3-mm-thick AA 6061 aluminum alloy sheet and 2-mm-thick Ti6Al4V titanium alloy sheet, which are both cut into 200-mm-long and 70-mm-wide pieces. The chemical compositions and mechanical properties of the two alloys are shown in Table I. Before welding, the surfaces of the alloys to be welded were polished with abrasive paper and degreased with acetone.

The setup of welding specimens is shown in Figure 1, where the Al alloy was placed on the Ti alloy during welding. The welding tool was made of W-Re alloy with a concave shoulder of 12 mm in diameter and a conical probe of 3.1 mm in length. The probe was mainly inserted in the Al alloy with a shoulder plunging depth of 0.1 mm. At room temperature, FSLW for Al/Ti dissimilar alloys was performed in air at various rotation speeds ranging from 800 to 1400 rpm under a constant welding speed of 100 mm/min and a tool tilting

angle of 3 deg. In addition, the temperature at the interface during welding was measured at a point that is 1.5 mm away from the weld center at the advancing side.

After welding, metallographic and tensile specimens were both cut from the joints vertically to the welding direction. The metallographic specimens were polished and then etched by Keller's etchant (1.0 mL HF + 1.5 mL HCl + 2.5 mL HNO$_3$ + 95 mL H$_2$O). The mean grain sizes were measured from the metallographs of the base materials and zones of the welds using image analysis software (Image Pro). Microstructure evolution of the joint was observed by an optical microscope (OM, DSX 510) and a scanning electron microscope (SEM, MERLIN Compact) equipped with an energy-dispersive X-ray spectrometer (EDS, OCTANE PLUS), which is used for analyzing the element distribution. Phase analysis was performed using X-ray diffraction (XRD, D/max 2500). Vickers hardness of the welded joints was tested perpendicular and parallel to the Al/Ti bonding interface using a microhardness tester (MICRO-586) with a load of 980 mN for 10 seconds on the joint cross section, as shown in Figure 2. Tensile shear tests were carried on three 20-mm-wide specimens for each joint using a tensile test machine (Instron 5967) with a crosshead speed of 1 mm/min at room temperature. The fracture surface morphology was examined by SEM.

III. RESULTS AND DISCUSSION

A. Macrographs of Joints at Various Rotation Speeds

The friction stir welds formed under the effect of violent friction between the pin tool and workpieces during welding, which is related with process parameters, friction, and the quality of FSW welds, can be improved though adjusting the parameters. As reported by Mishra and Ma,[17] for a given tool geometry and depth of penetration, the maximum welding temperature was a strong function of the rotation speed and the welding speed. The welding temperature was defined using the pseudo heat index w, as follows:

$$w = \frac{\omega^2}{v}, \qquad [1]$$

where w is the pseudo heat index and ω and v are the tool rotation speed (rpm) and welding speed (mm/min), respectively. The following equation explains the relation between the welding temperature (T, °C) and FSW parameters:

$$\frac{T_{max}}{T_{melting}} = K\left(\frac{\omega^2}{v \times 10^4}\right)^{\alpha}, \qquad [2]$$

where T_{max} is the maximum welding temperature (°C); $T_{melting}$ is the melting point of the base material (°C); ω and v are the tool rotation speed (rpm) and welding speed (mm/min), respectively; the exponent α was reported to range from 0.04 to 0.06; and the constant K is between 0.65 and 0.75.[17] It can be deduced that the increasing tool rotation speed leads to a higher

Table I. Chemical Compositions (Weight Percent) and Mechanical Properties of As-Received Materials

Fe	Al	Cu	Mg	Mn	Ti	V	Fe	Tensile Strength (MPa)	Elongation (Pct)
				Elements (Wt Pct)					
AA 6061	bal	0.67	1.31	0.59	—	—	—	345	9
Ti6Al4V	6.8	—	—	—	bal	4.5	0.3	895	10
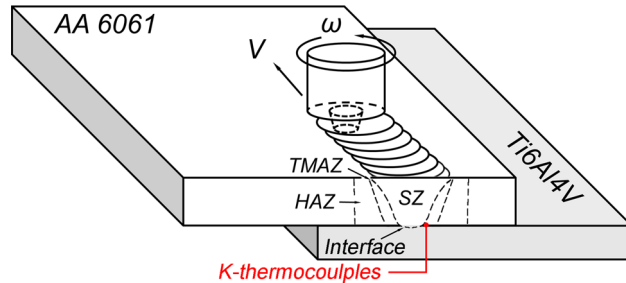
Fig. 1—Schematic illustration of FSLW of AA 6061 and Ti6Al4V alloys.
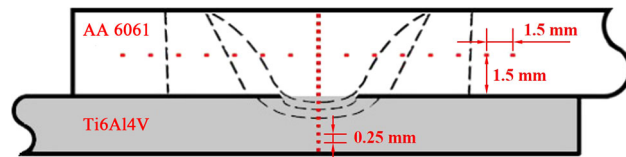
Fig. 2—Schematic illustration of the hardness test for the Al/Ti FSLW joint.

Fig. 3—Temperature history at the Al/Ti interface during FSLW.

temperature at a constant welding speed during FSW. The maximum temperature of Al/Ti FSLW in this study was calculated to range from 692 K to 785 K when the heat generated by the friction between the pin tool and Ti alloy was neglected. However, as shown in Figure 3, the measured temperature history at the interface during Al/Ti FSLW ranges from 744 K to 837 K, which is about 50 K higher than the calculated values. As mentioned previously, the pin tool was inserted 0.2 mm into the Ti alloy and the friction between the pin tool and Ti alloy contributed to the temperature enhancement.

The macrographs of the weld surfaces and cross sections of AA 6061/Ti6Al4V FSLW joints obtained at various rotation speeds ranging from 800 to 1400 rpm are shown in Figure 4. It is indicated that no visible defect can be found on the weld surface, as shown in Figure 4(a). However, peelings can be observed at the weld surfaces due to the relatively insufficient material flow with low heat input. Also, a smooth weld surface can be observed on Al alloy at 1400 rpm due to higher heat input and sufficient plastic flow of material. The appearance of the bonding interface between Al and Ti alloys varied when the rotation speed was increased, as shown in Figure 4(b). At a rotation speed within 1000 rpm, the heat input and mechanical effect were not sufficient to plasticize the Ti alloy; thus, a smooth interface with no obvious intermixing of material or
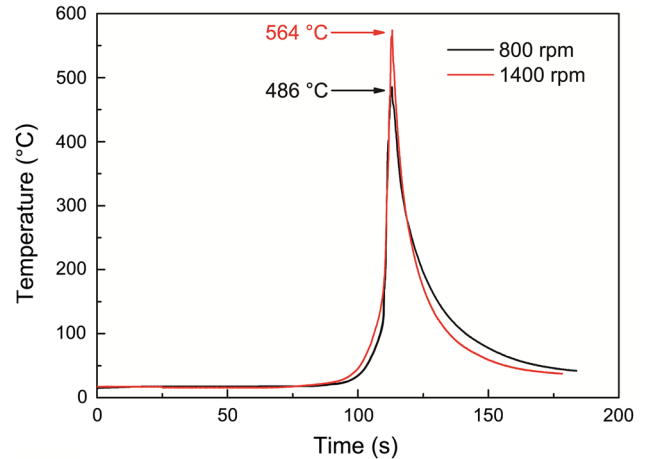
hook was obtained. When the rotation speed increased to over 1000 rpm, the Ti alloy was partly softened and entrapped into the Al alloy during welding due to more heat input and larger strain rate. As a result, obvious intermixing of Al and Ti alloys was found at the interface accompanied with the formation of hooks along the edge of the probe. It is interesting to note that the hook structure could only be found at the retreating side of the FSLW joint at 1200 rpm. When the rotation speed increased to 1400 rpm, hooks were formed at both sides of the joint because the Ti alloy was entrapped more into the Al alloy under the effect of more heat input and deformation.

B. Microstructure of the Typical Joint

Optical micrographs of the as-received Al and Ti alloys are shown in Figure 5. It is shown that AA 6061 alloy consists of α-Al and precipitations (Figure 5(a)), while a typical duplex microstructure composed of $\alpha + \beta$ phases can be observed in the Ti6Al4V alloy (Figure 5(b)). Metallographic characteristics of different areas in the joint welded at a rotation speed of 1200 rpm are shown in Figure 6. The FSLW joint, as shown in Figure 6(a), can be divided into the stir zone (SZ), thermomechanical affect zones ($TMAZ_{Al}$ and $TMAZ_{Ti}$), the heat affect zone (HAZ), the mix zone (MZ), and base metals (BMs). The grains in the HAZ grew to an average diameter slightly larger than that of the as-received Al alloy under the influence of the welding heat (Figure 6(b)). The grains in the $TMAZ_{Al}$ deformed and recrystallized due to dynamic recovery and
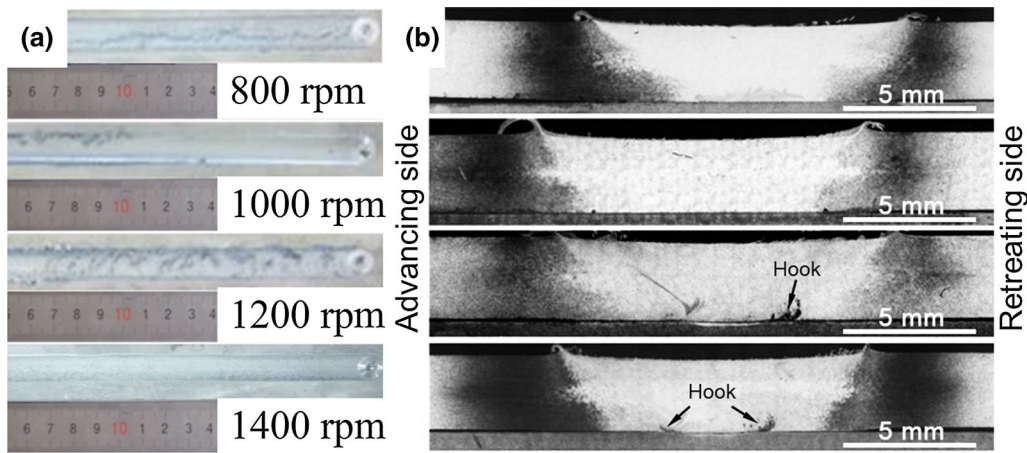
Fig. 4—Surface and cross section of the Al/Ti FSLW joints at various rotation speeds: (a) surface appearance of the welds and (b) cross sections of the welds.
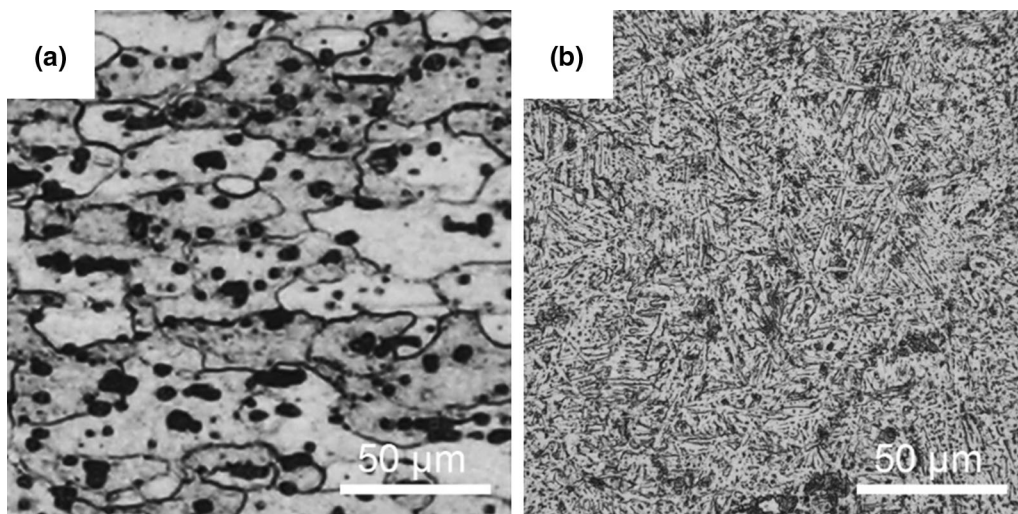

Fig. 5—OM micrographs of the as-received AA 6061 and Ti6Al4V alloys: (a) AA 6061 and (b) Ti6Al4V.

recrystallization as a consequence of the heat input and deformation during welding (Figure 6(c)). Additionally, there are deformed grains, which reveal the plastic flow of material during welding, in the TMAZ$_{Al}$. As they were heated and deformed severely during FSLW, the grains in the SZ dynamically recrystallized, which resulted in an SZ with refined equiaxed grains with an average grain size obviously smaller than that of the BM (Figure 6(d)). It should be noted that the Ti alloy was stirred into and mixed with Al alloy at the bottom of the SZ, resulting in the formation of the MZ at the interface (Figures 6(e) and (f)). In the MZ, the flow track reveals the intermixing of Al and Ti alloys. The TMAZ$_{Ti}$ is found beside the MZ at the Ti side as a consequence of the welding heat and deformation, which is in accordance with the investigations of Sanders et al.[18] Meanwhile, plasticized Ti alloy was also extruded into Al alloy along the probe edge, resulting in the formation of hook at the retreating side (Figure 6(g)). In addition, segregate Ti fragments were also stripped from the Ti alloy into the SZ along the material flow direction,

which is considered to be induced by the stirring and friction of the pin tool during FSLW.

C. Influence of Rotation Speed on Microstructure

The OM microstructure of the joints welded at 800 and 1400 rpm is shown in Figure 7. It is indicated that the microstructural evolution in the Al side of FSLW Al/Ti joints was strongly affected by rotation speed. The as-received Al alloy has a mean grain size of 10.63 μm, which is measured from Figure 5(a). However, the mean diameters of the grains in the welds were heavily affected by the rotation speed, as shown in Figure 7. The mean grain size of the grains in the SZ is 6.21 μm at 800 rpm, which is smaller than that of the SZ at 1400 rpm (7.55 μm). The grains in the TMAZ$_{Al}$ coarsened and deformed more significantly at 1400 rpm than at 800 rpm. The HAZ was only affected by the welding heat during FSLW, which resulted in a larger mean grain size than that of the BM. The mean grain size in the HAZ at 800 rpm is 11.89 μm compared with that of

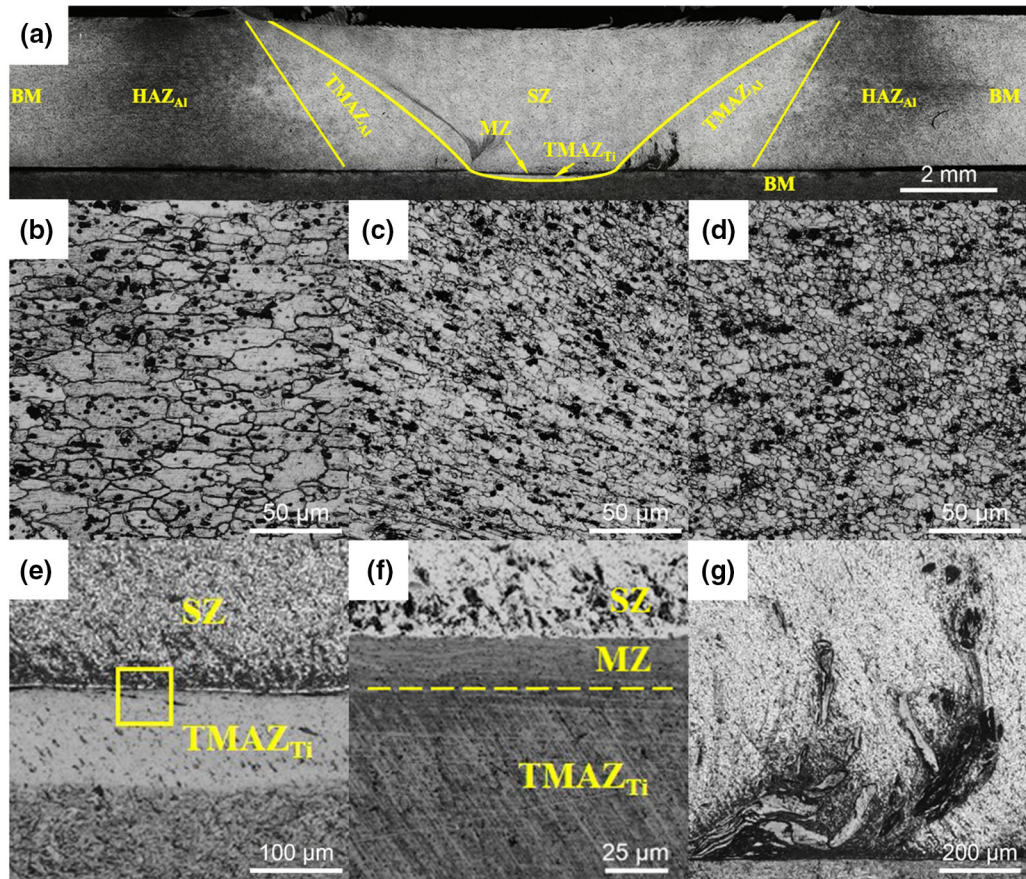Fig. 6—OM microstructure of the Al/Ti FSLW joint at 1200 rpm: (*a*) cross section, (*b*) middle of SZ, (*c*) TMAZ$_{Al}$, (*d*) HAZ$_{Al}$, (*e*) interface, (*f*) magnified image of Fig. 5(e), and (*g*) hook.
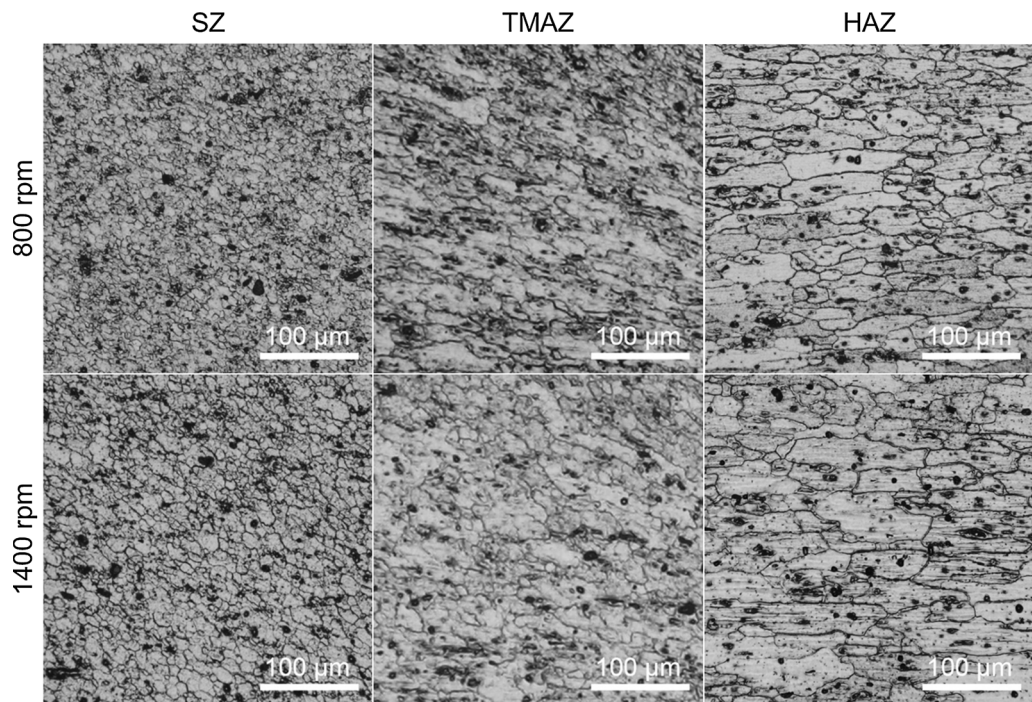

Fig. 7—OM microstructure at the Al side of the Al/Ti FSLW joints at 800 and 1400 rpm.

19.26 μm at 1400 rpm. It can be concluded that, during FSLW, lower rotation speed induced less welding heat, in accordance with Eq. [2], which leads to smaller grain size of the joint, as shown in Figure 8.

Microstructure and element distribution at the interface of Al/Ti FSLW joints were further observed by SEM and EDS, as shown in Figure 9. It is indicated that, instead of the intermixing of Al and Ti alloys, a relatively straight interface is observed in the joint welded at 800 rpm (Figure 9(a)), which is consistent with OM observation. However, the Ti alloy is significantly stirred into and mixed with the Al alloy in the MZ at 1400 rpm (Figure 9(b)) due to the enhanced heat input and plastic flow induced by high rotation speed. Meanwhile, the quantity of segregate Ti fragments entrapped into the Al alloy also increased with increasing rotation speed. It should be noted that, as shown in Figure 9(c), the element distribution varies continuously at the interface under 800 rpm, which indicates that the alloys are joined through diffusion. However, a 9-μm-thick diffusion layer can be observed at the interface when the rotation speed rose to 1400 rpm, as shown in Figure 9(d). Furthermore, continuous IMC layer can be observed at the boundary of the intermixed Al/Ti in the MZ. It is considered that TiAl$_3$ and TiAl can be formed in the MZ at 1400 rpm according to the EDS results shown in Figure 9(d) and Table II, which was in accordance with the investigation reported by Li et al.[11] It is reasonable that the content of Ti at the IMC layer increases as the layer locates deeper in the Ti alloy.

The EDS mapping results of the interface in Al/Ti FSLW joints obtained at 800 and 1400 rpm are shown in Figure 10. The Al/Ti interface is clear with no obvious intermixing of BMs for the joint obtained at 800 rpm, as shown in Figure 8(a), which is consistent with the SEM images discussed previously. According to the EDS mapping results, it can be determined that, at 1400 rpm, Ti not only diffused toward the Al alloy through the interface, but it also diffused and reacted with the intermixed Al alloy in the MZ. In addition, the solid solution or IMCs of Al-Ti can also form along the

edge of Ti fragments entrapped in the Al alloy near the interface, which can be explained by the uneven element distribution, heat input, and mechanical action during the nonequilibrium welding process. It is indicated that TiAl$_3$ was mainly formed at the Al/Ti interface and a small amount of TiAl can also be found in the MZ adjacent to the Ti alloy, according to the EDS results shown in Table II (Figures 9(d) and 10).

Five Al-Ti IMCs can be found from the Al-Ti phase diagram shown in Figure 11(a). Also, according to the standard free energy of formation (SFEF) shown in Figure 11(b), all these Al-Ti IMCs are able to form during FSLW due to their negative SFEF at welding temperature (744 K to 837 K). However, the formation of TiAl$_2$ and Ti$_2$Al$_5$ was based on the existence of TiAl. In addition, the formation of IMCs during the welding process is a transient nonequilibrium process, which cannot meet the requirements of the second-set reaction. Therefore, the two IMCs, Ti$_2$Al$_5$ and TiAl$_2$, can be omitted in our consideration. Moreover, it is obvious that TiAl$_3$ has the lowest SFEF among the other three Al-Ti IMCs. On the other hand, according to the effective heat of formation (EHF), which was first reported by Pretourius et al.[19] to predict the sequence of the IMC formation, the TiAl$_3$ was considered to be first formed in the Al-Ti reaction, as it has the lowest EHF at any Ti content, as shown in Figure 11(c), which was in accordance with the investigations by Chen and Nakata[13] and Sun et al.[20] Further, the TiAl can be formed after TiAl$_3$, as it has a lower EHF than the Ti$_3$Al when the content of Ti is no more than 78 at. pct.

The IMCs can be further observed at the hook, which was formed at the edge of the SZ, as shown in Figure 12. Also, the quantity of surrounding Ti fragments increased as the rotation speed rose to 1400 rpm. According to the EDS mapping results of the hook shown in Figure 12, it can be observed that the hook was mainly composed of the extruded Ti alloy, and IMCs can be observed at the boundary. Similarly, Al-Ti IMCs can be found along the edge of Ti fragments entrapped in Al alloy around the hook. It can be pointed out that the TiAl$_3$ and TiAl IMCs were formed around the hook according to EDS mapping results.

D. Hardness

The hardness distribution of the joints welded at various rotation speeds is shown in Figure 13. For the base materials, the hardness is about 340 HV on the Ti alloy and 110 HV on the Al alloy. The distribution of the hardness parallel to the interface at the center of the Al alloy is W shaped, as shown in Figure 13(a), which is in accordance with the investigations by Cui et al.[22] The hardness in the SZ decreased to 80 HV. Similarly, the hardness further declined in the TMAZ$_{Al}$ and reached the lowest value of 56 HV in the HAZ due to grain coarsening. The hardness distribution perpendicular to the Al/Ti interface is shown in Figure 13(b). The hardness of the Ti alloy declined to 307 HV at the TMAZ$_{Ti}$ and the hardness then increased to 360 HV at the interface due to the formation of IMCs, while the lowest hardness was also found in the SZ of the Al side.
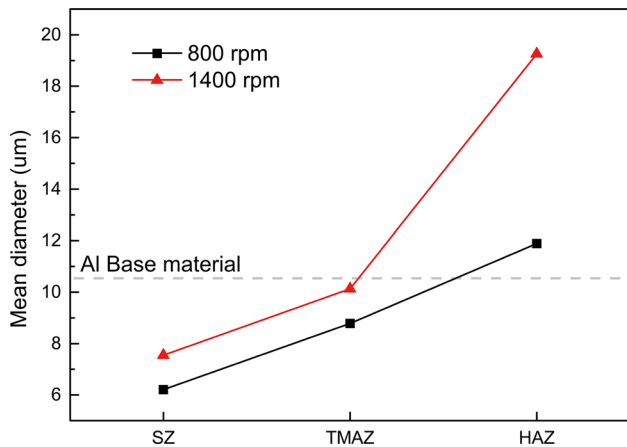

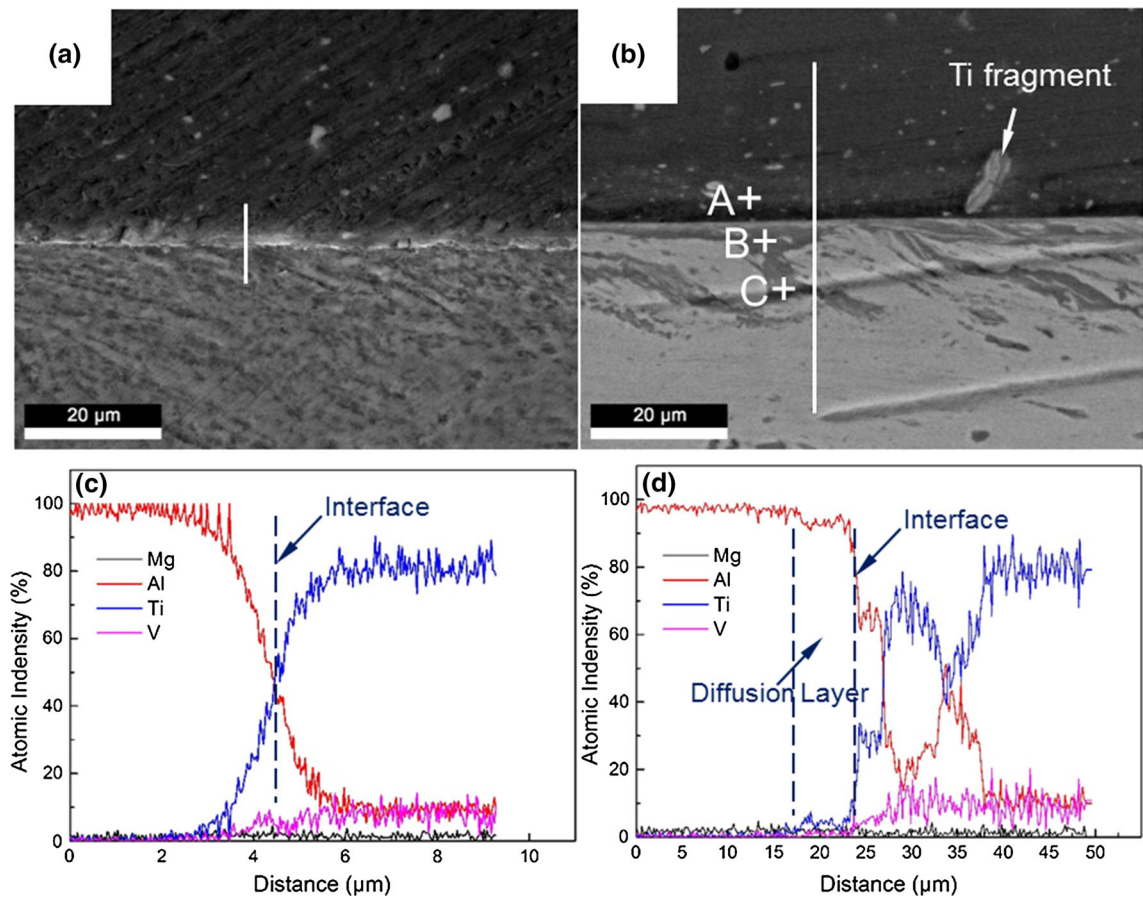Fig. 8—Mean grain diameter of different zones at the Al side at 800 and 1400 rpm.

Fig. 9—Micrographs and EDS linear images of the interface at 800 and 1400 rpm: (*a*) at 800 rpm, (*b*) at 1400 rpm, (*c*) EDS linear results in Fig. 7(a), and (*d*) EDS linear results in Fig. 7(b).

Table II. EDS Results of the Points Shown in Fig. 9(c) (Atomic Percent)

Points	Al	Ti	V	Mg	Phase
A	94.99	3.10	0.89	1.02	Al
B	73.26	25.88	0.86	0.70	TiAl$_3$
C	41.81	56.57	1.35	0.27	TiAl

The hardness variation in the Al/Ti FSLW joint can be attributed to the dynamic recrystallization and the solution of precipitations in Al alloy during FSLW. The hardness in the SZ is slightly higher than that in the TMAZ$_{Al}$ as a consequence of the smaller grains in the SZ. The larger strain rate enhanced the recrystallization of the grains as the rotation speed increased. However, the increased heat input promoted the growth of the grains and the dissolution of the precipitations. As a result, under the combination effect of heat and deformation, the hardness in the SZ and the TMAZ$_{Al}$ decreases with increasing rotation speed. In addition, the uneven distribution of grains and precipitations led to the variation of the hardness in the SZ and the TMAZ$_{Al}$. The HAZs were only heated without deformation during FSLW. The grains in the HAZ are overaged and the precipitations are partly dissolved, resulting in the lowest hardness of the Al/Ti FSLW joint. Also, the hardness in the HAZ also decreased with increasing rotation speed due to more heat input. It can be concluded that, during FSLW, a higher rotation speed leads to lower hardness as well as larger grain size in the joints. As for hardness distribution perpendicular to the Al/Ti interface, the hardness at the Ti alloy declined in the TMAZ$_{Ti}$. In regard to the interface, the hardness at the interface is higher than that of the as-received Ti alloy due to the formation of IMCs, as shown in Figure 12(b). It can be inferred that the rotation speed has relatively insignificant influence on the hardness distribution at the Ti side of the joint.

E. Tensile Shear Test

The tensile shear test results of the joints welded at various rotation speeds are shown in Figure 14. The maximum load of the FSLW joints at different rotation speeds reaches the maximum of 8984.8 N at 1000 rpm. It is found that the fracture of all test specimens happened around the interface. Although the IMCs are considered to embrittle the joints and reduce the tensile shear load, it is shown that an IMC layer with proper thickness can benefit the strength of the joint in the present study, which is in accordance with the
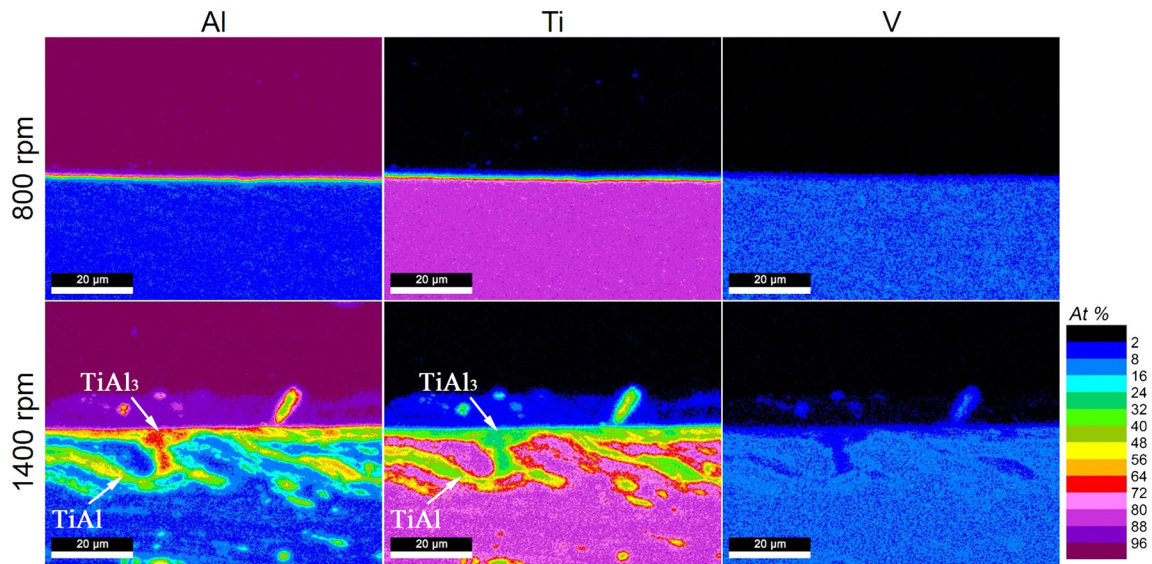
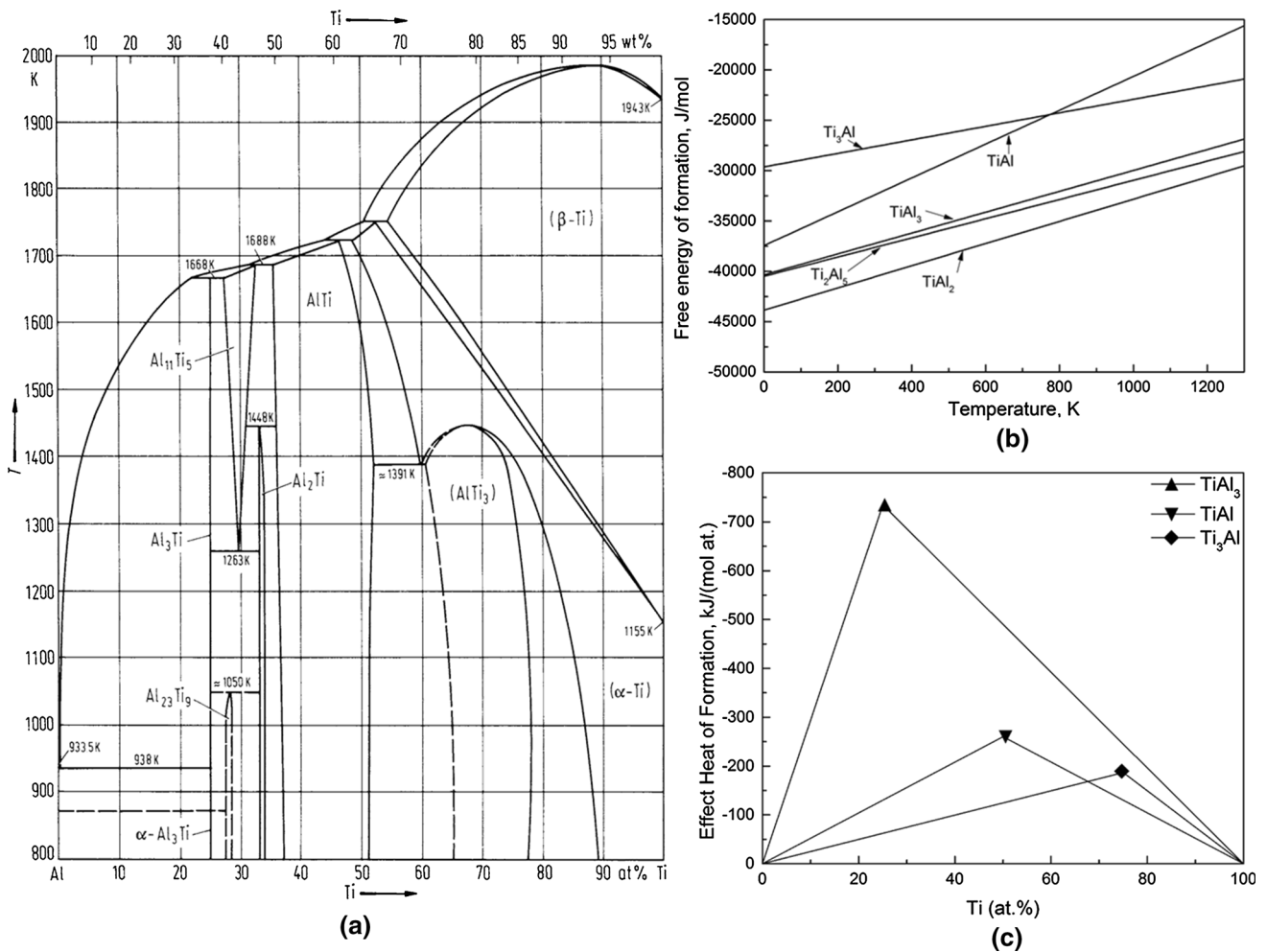Fig. 10—EDS mapping images of the interfaces at 800 and 1400 rpm.

Fig. 11—SFEF and EHF of the Al-Ti IMCs: (*a*) Al-Ti phase diagram,[21] (*b*) SFEF of the IMCs, and (*c*) EHF of the IMCs.
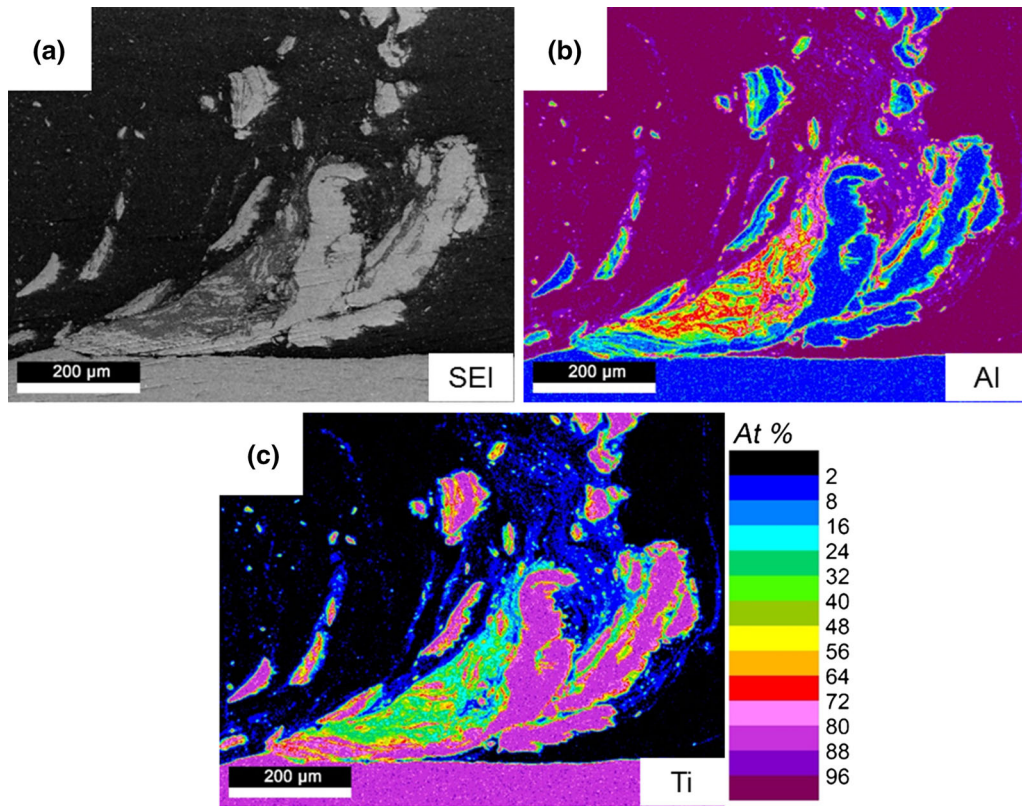
Fig. 12—Micrograph and EDS mapping images around the hook at 1400 rpm: (*a*) SEM image, (*b*) Al distribution, and (*c*) Ti distribution.
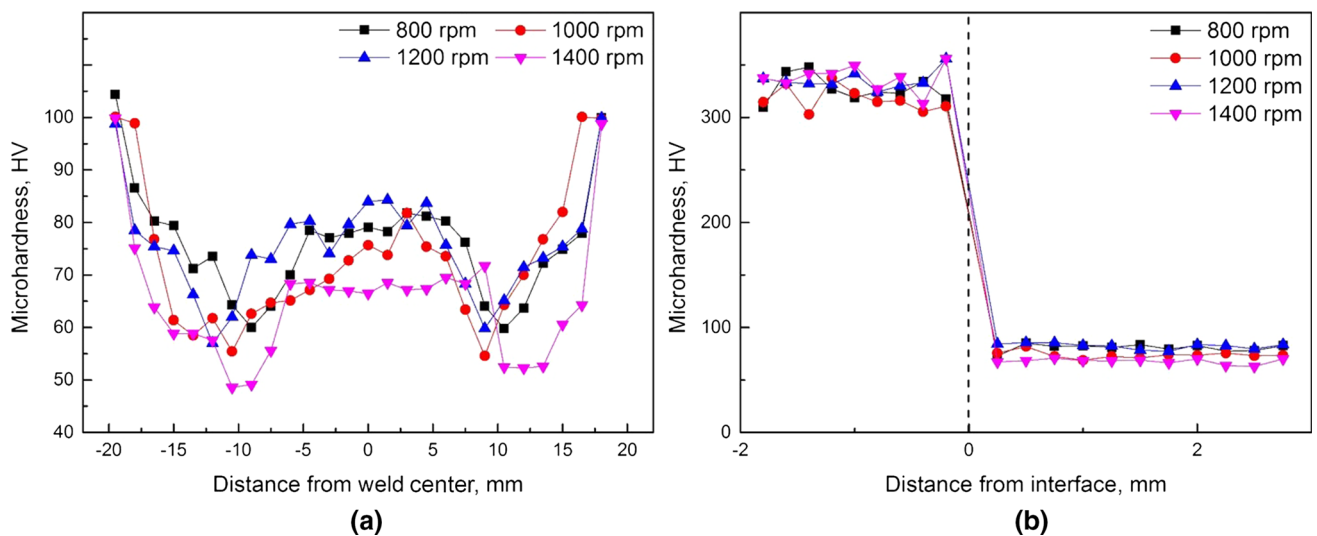

Fig. 13—Hardness distribution of the joints: (*a*) hardness profiles parallel to the interface and (*b*) hardness profiles perpendicular to the interface.

investigations reported by Pourali *et al.*[23] and Zhang *et al.*[24] As mentioned previously, more IMCs formed with increasing rotation speed. When the rotation speed is within 1000 rpm, the thickness of the IMC layers in the FSLW joints is less than the critical value, which results in the increasing load with increasing rotation speed. However, the joints failed at a lower load when increasing rotation speed exceeded 1000 rpm, which can

be explained by the thicker IMC layers and the formation of hook.

Macrographs of the corresponding fracture surface appearances of the failed joints are shown in Figure 15. It is obvious that the effective bonding width of the joints increases from 2.0 to 3.8 mm as the rotation speed rises to 1200 rpm from 800 rpm, and the bonding width remains about 3.8 mm when the rotation speed further

increases to 1400 rpm. If the failure energy of the interface is constant, a higher failure load can be reached with a wider joining area in the lap joint. However, the tendency of the failure load of the specimens at various rotation speeds did not agree with the tendency of the width of the joint, which revealed that the fractural mechanisms of the joints welded at various rotation speeds are different. The fracture surfaces of the joints welded at low rotation speed are smoother than the higher ones, and less Ti alloy is left on the Al side of the fractured surface at 800 rpm compared with that at 1400 rpm, which indicates less mechanical and metallurgical effect between Al and Ti alloys at low rotation speed. However, the superfluous mechanical and metallurgical effect between Al and Ti alloys at high rotation speed results in the formation of

excessive IMCs and hook, which can deteriorate the bearing capacity of the joint.

F. *Fracture Analysis*

The SEM micrographs and EDS mapping results on the cross sections of the fractured joints welded at 800 and 1400 rpm are shown in Figure 16. The joints all fractured around the Al-Ti interface. However, the joint at 800 rpm mainly fractured at the Al/Ti interface. It can be deduced that the interface of Al/Ti is weaker than the surrounding area due to insufficient heat input and deformation, which results in relatively weak mechanical-metallurgical bonding. As for the joint obtained at high rotation speed, Al and Ti alloys were intermixed and reacted around the interface, which led to a better mechanical-metallurgical bonded interface. However, once the IMCs formed over the proper content, the fractural mechanism changed as the maximum load decreased. As a result, the joint welded at 1400 rpm mainly fractured in the MZ, which reveals that the MZ is the weakest part in the joint obtained at 1400 rpm due to the superfluous formation of the Al-Ti IMCs.

The XRD spectra from the fracture surfaces at the Al side of the joints welded at 800 and 1400 rpm are shown in Figure 17. It can be observed that the fracture surface at the Al side in the joint at 800 rpm mainly consists of Al alloy and some Ti alloy, but no IMCs can be detected, as shown in Figure 17(a). As shown in Figure 17(b), the spectra of Ti, Al, and $TiAl_3$ can be found on the fracture surface of the joint welded at 1400 rpm. Although TiAl can be found in the EDS results, TiAl cannot be found in the XRD results due to its small quantity. The appearance of the IMCs on the fracture surface reveals that the fracture of the joints can start with the microcracks formed at the brittle IMCs and then result in break, and the complex IMC layers weaken the friction stir lap welded dissimilar joints of AA 6061 and Ti6Al4V alloys under high rotation speed.
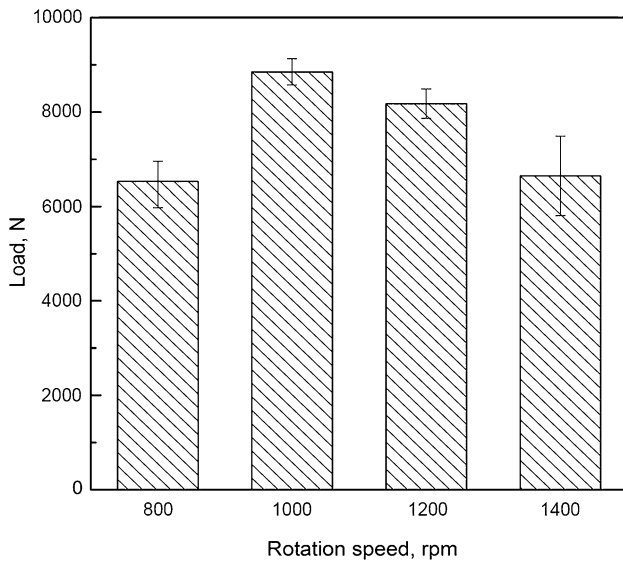

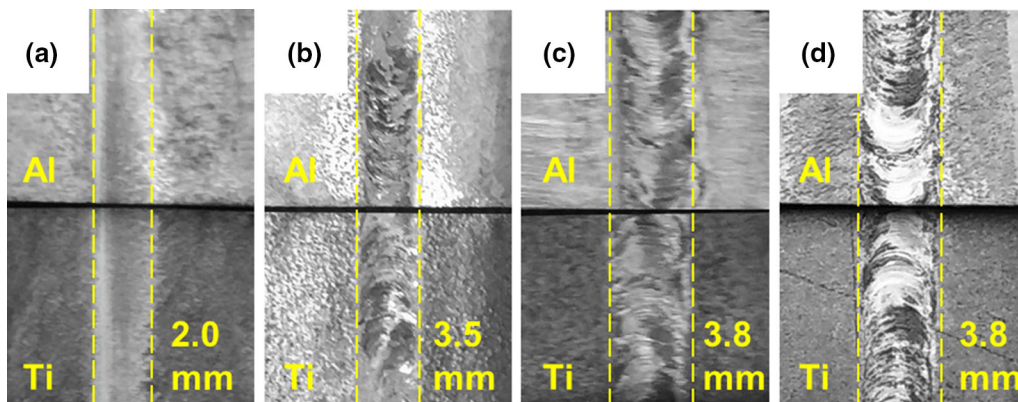Fig. 14—Tensile shear test results of the Al/Ti lap joints.

Fig. 15—Fracture surfaces of the failed specimens for (*a*) 800 rpm, (*b*) 1000 rpm, (*c*) 1200 rpm, and (*d*) 1400 rpm.
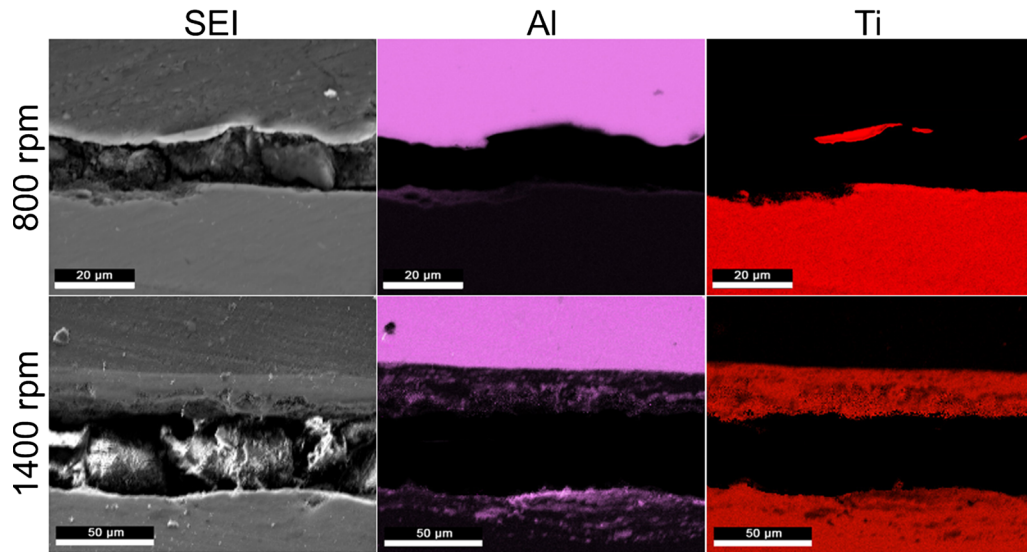
Fig. 16—SEM profile and EDS mapping results of the fractured specimens for 800 and 1400 rpm.
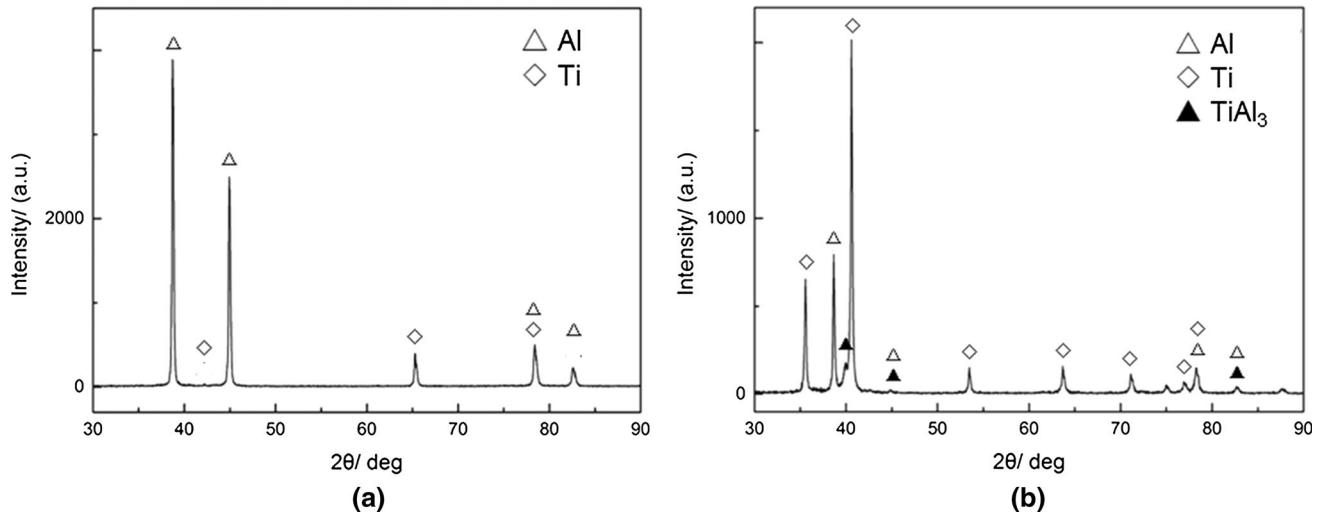

Fig. 17—XRD results of the fracture surface of different joints: (*a*) 800 rpm and (*b*) 1400 rpm.

The fracture surfaces are similar at various rotation speeds; thus, the SEM micrographs of the typical fracture surface morphology of the joint obtained at 1200 rpm are shown in Figure 18. As mentioned previously, the Al and Ti alloys were both left on the fracture surfaces of the opposite sides of the joint during the tensile shear test. Further, there are some differences in the micrographs of the fracture surfaces of the Al and Ti sides. As shown in Figure 18(a), the fracture surface at the Al side is featured by shallow dimples, indicating that the fracture on the local part of Al alloy has the characteristics of ductile failure. Otherwise, the cleavage planes and tearing ridge, which are the characteristics of brittle fracture, can be identified at the fracture surface of the Ti side, as shown in Figure 18(b). In addition, tiny oxides, which are considered to be Al_2O_3 according to the EDS result, can also be observed at the fracture surface of the Ti side due to the reaction between Al and

air under the effect of heat input during welding, as shown in Figure 18(c).

IV. CONCLUSIONS

FSLW of the AA 6061 aluminum alloy and T6Al4 V titanium alloy was conducted. The microstructure and mechanical properties of the lap joints were investigated. Defect-free joints can be obtained at various rotation speeds ranging from 800 to 1400 rpm for Al/Ti FSLW. The joint can be divided into SZ, MZ, $TMAZ_{Al}$ and $TMAZ_{Ti}$, and HAZ. No Al/Ti intermixing can be observed at the interface in the joint obtained at the rotation speed of 800 rpm, but diffusion between Al/Ti occurred with no obvious layer. When the rotation speed rose to 1400 rpm, a 9-μm-thick diffusion layer near the Al side, as well as the Al/Ti intermixing and
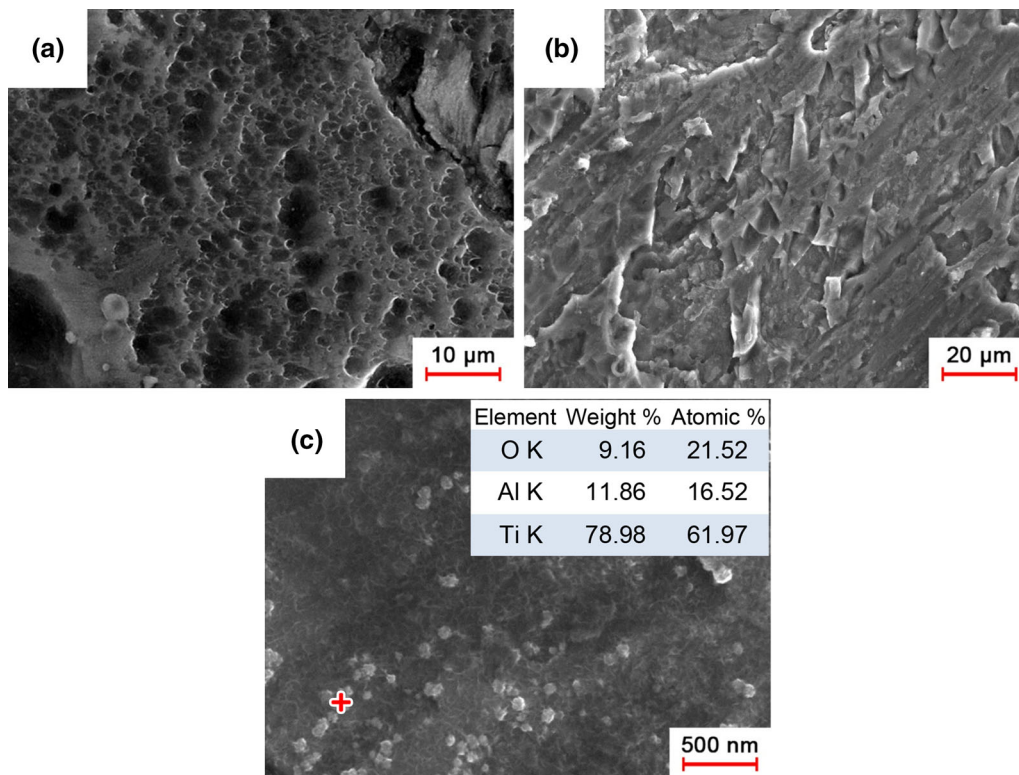
Element	Weight %	Atomic %
O K	9.16	21.52
Al K	11.86	16.52
Ti K	78.98	61.97

Fig. 18—SEM micrographs of the fracture surface: (*a*) Al side, (*b*) Ti side, and (*c*) oxides on the Ti side.

hooks, was formed around the interface. The IMCs of $TiAl_3$ and TiAl were considered to form within the MZ as well as at the edge of hooks and the surrounding Ti fragments. The hardness distribution on the Ti side of the joint decreased to 307 HV at the $TMAZ_{Ti}$ and then reached the maximum at about 360 HV at the interface. The maximum failure load of 8985 N of tensile shear test specimens can be reached at 1000 rpm. The joint welded at 800 rpm fractured at the Al/Ti interface, and a small amount of $TiAl_3$ can be found on the fracture surface. As the rotation speed rose to 1400 rpm, the specimens fractured at the MZ along the Ti-Al IMC layer. Both $TiAl_3$ and TiAl can be depicted from the XRD spectra of fracture surfaces. Cleavage planes and dimples can be found on the fracture surface of the Al and Ti sides of joints obtained as the rotation speed varied.

REFERENCES

1. M. Simoncini and A. Forcellese: *Mater. Des.*, 2012, vol. 41, pp. 50–60.
2. K. Michael, W. Florian, and V. Frank: *Opt. Las. Eng.*, 2005, vol. 43, pp. 1021–35.
3. S.X. Lv, Q.L. Cui, X.J. Huang, and X.J. Jing: *Mater. Sci. Eng. A*, 2013, vol. 568, pp. 150–54.
4. S.H. Chen, L.Q. Li, Y.B. Chen, and D.J. Liu: *Trans. Nonferrous Met. Soc. China*, 2010, vol. 20, pp. 64–70.
5. S.Y. Chang, L.C. Tsao, Y.H. Lei, S.M. Mao, and C.H. Huang: *J. Mater. Process. Technol.*, 2012, vol. 212, pp. 8–14.
6. A.N. Alhazaa and T.I. Khan: *J. Alloys Compds.*, 2010, vol. 494, pp. 351–58.
7. S.Q. Wang, V.K. Patel, S.D. Bhole, G.D. Wen, and D.L. Chen: *Mater. Des.*, 2015, vol. 78, pp. 33–41.
8. C.Q. Zhang, J.D. Robson, and P.B. Prangnell: *J. Mater. Process. Technol.*, 2016, vol. 231, pp. 382–88.
9. M. Aonuma and K. Nakata: *Mater. Trans.*, 2011, vol. 52, pp. 948–52.
10. A. Wu, Z. Song, K. Nakata, J. Liao, and L. Zhou: *Mater. Des.*, 2015, vol. 71, pp. 85–92.
11. B. Li, Z. Zhang, Y. Shen, W. Hu, and L. Luo: *Mater. Des.*, 2014, vol. 53, pp. 838–48.
12. K.S. Bang, K.J. Lee, H.S. Bang, and H.S. Bang: *Mater. Trans.*, 2011, vol. 52, pp. 974–78.
13. Y.C. Chen and K. Nakata: *Mater. Des.*, 2009, vol. 30, pp. 469–74.
14. Y.H. Chen, Q. Ni, and L.M. Ke: *Trans. Nonferrous Met. Soc. China*, 2012, vol. 22, pp. 299–304.
15. B. Li, Y. Shen, L. Luo, W. Hu, and Z. Zhang: *Mater. Des.*, 2013, vol. 49, pp. 647–56.
16. Z.W. Chen and S. Yazdanian: *Mater. Sci. Eng. A*, 2015, vol. 634, pp. 37–45.

17. R.S. Mishra and Z.Y. Ma: *Mater. Sci. Eng.: R: Rep.*, 2005, vol. 50, pp. 13–58.
18. D.G. Sanders, P. Edwards, A.M. Cantrell, K. Gangwar, and M. Ramulu: *JOM*, 2015, vol. 67 (5), pp. 1054–62.
19. R. Pretorius, T.K. Marais, and C.C. Theron: *Mater. Sci. Eng. R*, 1993, vol. 10 (1–2), pp. 61–83.
20. Q.J. Sun, J.Z. Li, Y.B. Liu, B.P. Li, P.W. Xu, and J.C. Feng: *Mater. Des.*, 2017, vol. 116, pp. 316–24.
21. ASM International: *Binary Alloy Phase Diagrams*, 2nd ed., ASM International, Novelty, 1990, vol. 1, p. 233.
22. L. Cui, X. Yang, G. Zhou, X. Xu, and Z. Shen: *Mater. Sci. Eng. A*, 2012, vol. 543, pp. 58–68.
23. M. Pourali, A. Abodollah-zadeh, T. Saeid, and F. Kargar: *J. Alloys Compds.*, 2017, vol. 715, pp. 1–8.
24. Q. Zhang, X. Feng, Y. Shen, G. Huang, and P. Zhao: *J. Alloys Compds.*, 2017, vol. 695, pp. 952–61.